Journal of Contaminant Hydrology 181 (2015) 102–113

Contents lists available at ScienceDirect

Journal of Contaminant Hydrology

journal homepage: www.elsevier.com/locate/jconhyd

Modeling dense-colloid and virus cotransport in three-dimensional porous media

Vasileios E. Katzourakis [a], Constantinos V. Chrysikopoulos [b,*]

[a] Environmental Engineering Laboratory, Civil Engineering Department, University of Patras, Patras 26500, Greece
[b] School of Environmental Engineering, Technical University of Crete, Chania 73100, Greece

ARTICLE INFO

Article history:
Received 2 December 2014
Received in revised form 16 May 2015
Accepted 22 May 2015
Available online 29 May 2015

Keywords:
Viruses
Dense colloids
Cotransport
Mathematical modeling
Porous media
Gravity effects

ABSTRACT

A three-dimensional numerical model was developed to investigate the simultaneous transport (cotransport) of dense colloids and viruses in homogeneous, water saturated, porous media with horizontal uniform flow. The dense colloids are assumed to exist in two different phases: suspended in the aqueous phase, and attached reversibly and/or irreversibly onto the solid matrix. The viruses are assumed to exist in four different phases: suspended in aqueous phase, attached onto the solid matrix, attached onto suspended colloids, and attached onto colloids already attached onto the solid matrix. The viruses in each of the four phases are assumed to undergo inactivation with different rates. Moreover, the suspended dense colloids as well as viruses attached onto suspended dense colloids are assumed to exhibit a "restricted" settling velocity as a consequence of the gravitational force; whereas, viruses due to their small sizes and densities are assumed to have negligible "restricted" settling velocity. The governing differential equations were solved numerically with the finite difference schemes, implicitly or explicitly implemented. Model simulations have shown that the presence of dense colloid particles can either enhance or hinder the horizontal transport of viruses, but also can increase the vertical migration of viruses.

1. Introduction

The transport of biocolloids (viruses, bacteria, protozoa) in aquifers has received considerable attention by numerous environmental engineers and hydrogeologists, because waterborne disease outbreaks are often connected directly to groundwater contamination (Craun et al., 2010). Biocolloids can be found present in groundwater due to accidental wastewater releases, broken sewer lines, septic tanks, agricultural practices, sanitary landfills, and artificial groundwater recharge activities (Anders and Chrysikopoulos, 2005; Chrysikopoulos et al., 2010; Chu et al., 2003; Masciopinto et al., 2008; Sim and Chrysikopoulos, 2000). The transport of biocolloids in the subsurface is affected by several factors including water chemistry, water saturation level, interstitial velocity, attachment onto the solid matrix and suspended colloid particles, grain size, biocolloid size, inactivation, temperature, and gravitational settling (Anders and Chrysikopoulos, 2006; Chen and Bai, 2012; Chen et al., 2010; Chrysikopoulos and Aravantinou, 2012, 2014; Jin et al., 1997; Kim et al., 2009; Ma et al., 2011; Syngouna and Chrysikopoulos, 2011; Torkzaban et al., 2008; Wan et al., 1995). Colloids, which are naturally occurring in groundwater as a result of precipitation of supersaturated phases, well drilling, dissolution of cementing agents, and leaching from the unsaturated zone (Compere et al., 2001; Gschwend et al., 1990), can serve as carriers that either hinder or enhance the transport of dissolved pollutants, and suspended biocolloids, depending on the physicochemical conditions of the aquifer (Abdel-Salam and Chrysikopoulos, 1995a; Artinger et al., 2002; James et al., 2005; Kretzschmar et al., 1999; McCarthy, 1998; McGechan and Lewis, 2002; Mibus et al., 2007; Ouyang et al., 1996; Saiers and Hornberger, 1996; Sen and Khilar, 2006; Severino et al., 2007; Syngouna and Chrysikopoulos, 2013, 2015; Tatalovich et al., 2000; Villholth et al., 2000; Walshe et al., 2010).

* Corresponding author. Fax: +30 28210 37847.
E-mail address: cvc@enveng.tuc.gr (C.V. Chrysikopoulos).

http://dx.doi.org/10.1016/j.jconhyd.2015.05.010
0169-7722/

Several analytical and numerical one- and three-dimensional models for biocolloid transport (Anders and Chrysikopoulos, 2009; Bradford et al., 2011; Chrysikopoulos and Sim, 1996; Chrysikopoulos et al., 2012; Harvey and Garabedian, 1991; Park et al., 1992; Sim and Chrysikopoulos, 1995, 1996, 1998; Tim and Mostaghimi, 1991) as well as colloid and biocolloid cotransport in porous media (Katzourakis and Chrysikopoulos, 2014; Vasiliadou and Chrysikopoulos, 2011) are available in the literature. However, the collection of mathematical models for transport of dense colloids in porous media is limited (e.g. Chrysikopoulos and Syngouna, 2014; Flowers and Hunt, 2007).

The objective of the present study was to improve the three-dimensional colloid and virus cotransport mathematical model developed by Katzourakis and Chrysikopoulos (2014), and further extend it to account for "restricted" dense-colloid settling, as suggested by Chrysikopoulos and Syngouna (2014). To our knowledge, a mathematical model describing the cotransport of dense-colloids and viruses in three-dimensional water saturated, homogeneous porous media under uniform horizontal flow, accounting for "restricted" settling of dense colloids has not been previously presented in the literature.

2. Mathematical modeling

The cotransport mathematical model proposed in this work consists of two governing partial differential equations (PDEs), and a set of initial and boundary conditions. The first PDE describes the transport of dense colloids and is based on previous works by Sim and Chrysikopoulos (1998, 1999), Katzourakis and Chrysikopoulos (2014), Wan et al. (1995), and Chrysikopoulos and Syngouna (2014). The second PDE describes the transport of viruses in the presence of the dense colloids and is based on previous works by Abdel-Salam and Chrysikopoulos (1995a,b), Bekhit et al. (2009), Vasiliadou and Chrysikopoulos (2011), Katzourakis and Chrysikopoulos (2014), with additional modifications to account for settling of dense colloids in porous media ("restricted" settling). Note that the proposed mathematical model assumes that the dense colloids, which undergo "restricted" settling, can be either suspended in the aqueous phase, C_c [M_c/L^3], or attached onto the solid matrix, C_c^* [M_c/M_s]. Furthermore, the mathematical model assumes that viruses can be suspended in the aqueous phase, C_v [M_v/L^3], attached onto suspended colloids, C_{vc} [M_v/M_c], attached onto the solid matrix, C_{v^*} [M_v/M_s], and attached onto colloids already attached onto the solid matrix, $C_{v^*c^*}$ [M_v/M_c]. Note that the subscripts c, v, and vc represent colloid, virus and virus–colloid, respectively. Also, M_c represents the mass of colloids, M_v the mass of viruses, and M_s the mass of the solid matrix. The six different concentrations accounted for in the new mathematical model are depicted graphically in Fig. 1.

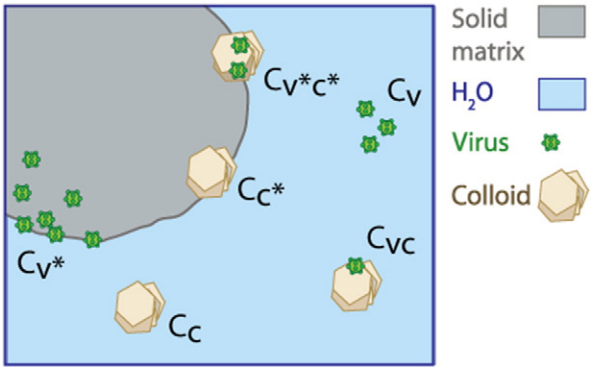

Fig. 1. Schematic illustration of the various concentrations accounted for in the cotransport numerical model.

The transport of dense colloid particles in three-dimensional, water saturated, homogeneous porous media with one-directional uniform flow, accounting for colloid gravity effects and kinetic attachment onto the solid matrix, is governed by the following partial differential equation (Chrysikopoulos and Syngouna, 2014; Sim and Chrysikopoulos, 1998):

$$\frac{\partial C_c(t,x,y,z)}{\partial t}+\frac{\rho_b}{\theta}\frac{\partial C_{c^*}(t,x,y,z)}{\partial t}-D_{xc}\frac{\partial^2 C_c(t,x,y,z)}{\partial x^2}-D_{yc}\frac{\partial^2 C_c(t,x,y,z)}{\partial y^2}-D_{zc}\frac{\partial^2 C_c(t,x,y,z)}{\partial z^2}+\left(U_x+U_{cs(\pm i)}\right)\frac{\partial C_c(t,x,y,z)}{\partial x}+U_{cs(-k)}\frac{\partial C_c(t,x,y,z)}{\partial z}=F_c(t,x,y,z) \quad (1)$$

where t [t] is time; x [L] is the Cartesian coordinate in the longitudinal direction; y [L] is the Cartesian coordinate in the lateral direction; z [L] is the Cartesian coordinate in the vertical direction; ρ_b [M_s/L^3] is the bulk density of the solid matrix; θ [–] is the porosity of the porous medium; D_{xc}, D_{yc}, D_{zc} [L^2/t] are the longitudinal, lateral, and vertical hydrodynamic dispersion coefficients of the suspended colloids, respectively; F_c [M_c/L^3t] is a general form of the colloid source configuration; U_x [L/t] is the average interstitial velocity along the x-direction; and $U_{cs(\pm i)}$ [L/t] and $U_{cs(-\mathbf{k})}$ [L/t] are the $\pm$x-directional and negative z-directional components of the "restricted particle" settling velocity (in porous media), which is just a modification of the "free particle" settling velocity, commonly used in static water columns (Russel et al., 1989), applicable to granular porous media (Chrysikopoulos and Syngouna, 2014):

$$U_{cs(\pm i)}=f_s\frac{\left(\rho_p-\rho_w\right)d_p^2}{18\mu_w}g_{(\pm i)} \quad (2a)$$

$$U_{cs(-k)}=f_s\frac{\left(\rho_p-\rho_w\right)d_p^2}{18\mu_w}g_{(-k)} \quad (2b)$$

where f_s [–] is the correction factor accounting for particle settling in the presence of the solid matrix of granular porous media; ρ_w [M/L^3] is the density of the suspending fluid (water); ρ_p [M/L^3] is the density of the colloid particle; μ_w [$M/(L\cdot t)$] is the dynamic viscosity of water; and $g_{(\pm i)}$ [L/t^2] and $g_{(-\mathbf{k})}$ [L/t^2] are the x-directional and z-directional components of the gravity vector defined as:

$$g_{(\pm i)}=g\cos\beta \quad (3a)$$

$$g_{(-k)}=-g\sin\beta \quad (3b)$$

where g [M/t^2] is the acceleration due to gravity; β [°] is the angle of the main flow direction (x-direction) with respect to the direction of gravity ($0° \le \beta \le 180°$); $\pm\mathbf{i}$ and $-\mathbf{k}$ are the unit vectors parallel ($\pm$x-direction) and perpendicular (negative z-direction) to the flow, respectively (see Fig. 2); f_s is the

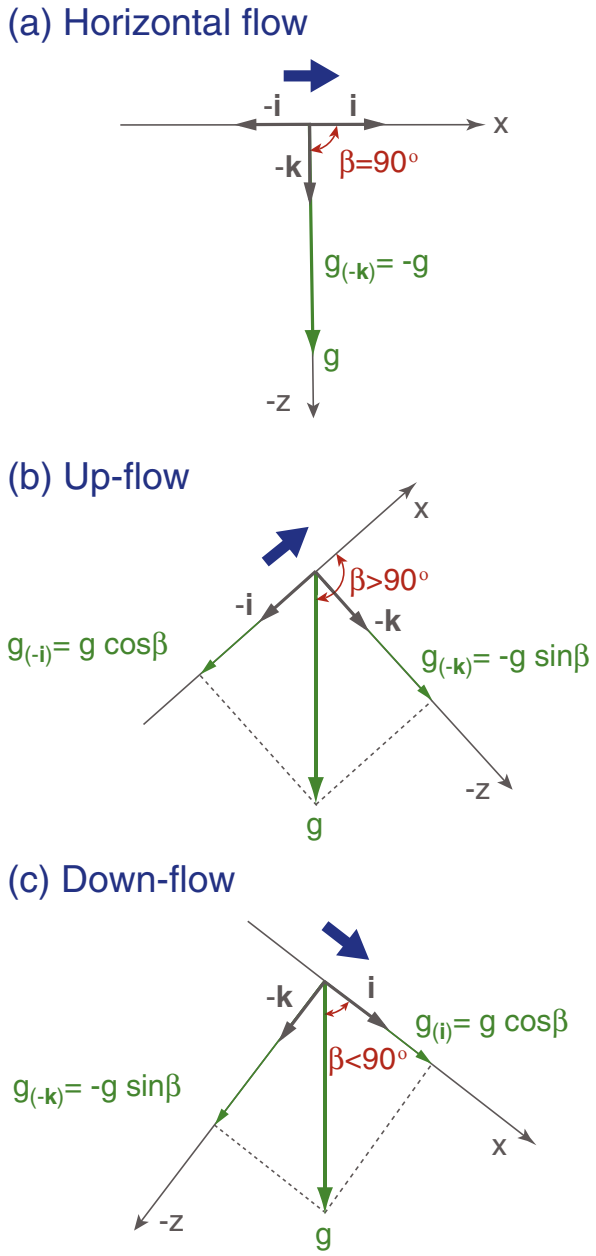

Fig. 2. Schematic illustration of the gravity vector components for: (a) horizontal flow, (b) up-flow, and (c) down-flow conditions. The angle β (0° ≤ β ≤ 180°) is between the main flow direction (x-direction) and the direction of gravity.

correction factor which allows the calculation of the average sedimentation based on the free average particle sedimentation velocity, through water saturated porous media (Wan et al., 1995):

$$f_s = \frac{b + 0.67}{b + 0.93/\varepsilon} \tag{4}$$

where $b \approx 1$ is the average free settling segment length to the grain radius ratio, and ε ($0 \le \varepsilon \le 1$) is a correction factor that takes into account the effect of the grain surface onto the settling velocity. Also $f_s \approx 0.9$ when the existing grains found on the solid surface of the porous medium do not add additional frictional resistance, but only contribute to the tortuosity (Wan et al., 1995). Colloids attached onto the solid matrix, C_{c^*}, are assumed to be reversibly, $C_{c^*}^{(r)}$ [M_c/M_s], and/or irreversibly, $C_{c^*}^{(i)}$ [M_c/M_s], attached. Consequently, the concentration of colloids attached onto the solid matrix can be represented as (Katzourakis and Chrysikopoulos, 2014):

$$C_{c^*} = C_{c^*}^{(r)} + C_{c^*}^{(i)}. \tag{5}$$

Also, the corresponding colloid accumulation term in Eq. (1) can be expressed as:

$$\frac{\rho_b}{\theta}\frac{\partial C_{c^*}(t,x,y,z)}{\partial t} = \frac{\rho_b}{\theta}\left[\frac{\partial C_{c^*}^{(r)}(t,x,y,z)}{\partial t} + \frac{\partial C_{c^*}^{(i)}(t,x,y,z)}{\partial t}\right]. \tag{6}$$

The reversible accumulation term is given by (Sim and Chrysikopoulos, 1998, 1999):

$$\frac{\rho_b}{\theta}\frac{\partial C_{c^*}^{(r)}(t,x,y,z)}{\partial t} = r_{c\text{-}c^{*(r)}} C_c(t,x,y,z) - r_{c^{*(r)}\text{-}c}\frac{\rho_b}{\theta} C_{c^*}^{(r)}(t,x,y,z) \tag{7}$$

where $r_{c\text{-}c^{*(r)}}$ [1/t] is the forward rate coefficient of colloid attachment onto the solid matrix, and $r_{c^{*(r)}\text{-}c}$ [1/t] is the reverse rate coefficient of colloid detachment from the solid matrix. The irreversible accumulation term is given by (Compere et al., 2001):

$$\frac{\rho_b}{\theta}\frac{\partial C_{c^*}^{(i)}(t,x,y,z)}{\partial t} = r_{c\text{-}c^{*(i)}} C_c(t,x,y,z) \tag{8}$$

where $r_{c\text{-}c^{*(i)}}$ is the forward rate coefficient of irreversible colloid attachment onto the solid matrix.

The three-dimensional virus transport in water saturated, homogeneous porous media with one-directional uniform flow, accounting for virus attachment onto suspended dense colloid particles, the solid matrix, and colloid particles already attached onto the solid matrix, first-order inactivation of suspended and attached viruses, and gravity effects, is governed by the following partial differential equation (Abdel-Salam and Chrysikopoulos, 1995a,b; Katzourakis and Chrysikopoulos, 2014; Vasiliadou and Chrysikopoulos, 2011):

$$\begin{aligned}\frac{\partial}{\partial t}\left(C_v + \frac{\rho_b}{\theta}C_{v^*} + C_c C_{vc} + \frac{\rho_b}{\theta}C_{c^*}C_{v^*c^*}\right) &= D_{xv}\frac{\partial^2 C_v}{\partial x^2} + D_{xvc}\frac{\partial^2}{\partial x^2}(C_c C_{vc}) \\ &+ D_{yv}\frac{\partial^2 C_v}{\partial y^2} + D_{yvc}\frac{\partial^2}{\partial y^2}(C_c C_{vc}) + D_{zv}\frac{\partial^2 C_v}{\partial z^2} + D_{zvc}\frac{\partial^2}{\partial z^2}(C_c C_{vc}) \\ &- \left(U_x + U_{vs(\pm i)}\right)\frac{\partial}{\partial x}(C_v + C_c C_{vc}) - U_{vs(-k)}\frac{\partial}{\partial z}(C_v) \\ &- U_{vcs(-k)}\frac{\partial}{\partial z}(C_c C_{vc}) - \lambda_v C_v - \lambda_{vc} C_v C_{vc} - \lambda_{v^*}\frac{\rho_b}{\theta}C_{v^*} \\ &- \lambda_{v^*c^*}\frac{\rho_b}{\theta}C_{c^*}C_{v^*c^*} + F_v(t,x,y,z)\end{aligned} \tag{9}$$

where D_{xv}, D_{yv}, D_{zv} [L^2/t] are the longitudinal, lateral, and vertical hydrodynamic dispersion coefficients of the suspended viruses, respectively; D_{xvc}, D_{yvc}, D_{zvc} [L^2/t] are the longitudinal, lateral, and vertical hydrodynamic dispersion

coefficients of viruses attached onto suspended colloids, respectively; λ_v [1/t] is the decay rate of the suspended viruses in aqueous phase; λ_{v^*} [1/t] is the decay rate of attached viruses onto the solid matrix; λ_{vc} [1/t] is the decay rate of suspended virus–colloid particles in aqueous phase; $\lambda_{v^*c^*}$ [1/t] is the decay rate of attached virus–colloid particles onto the solid matrix; F_v [M_v/L^3t] is a general form of the virus source configuration; $U_{vs(-\mathbf{k})}$ [L/t] is "restricted" settling velocity of the viruses; and $U_{vcs(-\mathbf{k})}$ [L/t] is "restricted" settling velocity of the virus–colloid complexes. Note that in this study viruses are considered to be very small particles and their "restricted" settling velocity is assumed to be equal to zero ($U_{vs(\pm\mathbf{i})} = U_{vs(-\mathbf{k})} = 0$). Also, it is assumed that virus–colloid complexes and colloid particles have the same "restricted" settling velocity ($U_{vcs(-\mathbf{k})} = U_{cs(-\mathbf{k})}$).

The second accumulation term on the left hand side of Eq. (9) is given by (Sim and Chrysikopoulos, 1998,1999):

$$\frac{\rho_b}{\theta}\frac{\partial C_{v*}(t,x,y,z)}{\partial t} = r_{v\text{-}v^*}C_v(t,x,y,z) - r_{v^*\text{-}v}\frac{\rho_b}{\theta}C_{v^*}(t,x,y,z) - \lambda_{v^*}\frac{\rho_b}{\theta}C_{v^*}(t,x,y,z) \tag{10}$$

where $r_{v\text{-}v^*}$ [1/t] is the rate coefficient of virus attachment onto the solid matrix; and $r_{v^*\text{-}v}$ [1/t] is the rate coefficient of virus detachment from the solid matrix. The third accumulation term on the left hand side of Eq. (9) is given by (Bekhit et al., 2009; Katzourakis and Chrysikopoulos, 2014):

$$\frac{\partial}{\partial t}(C_cC_{vc}) = r_{v-vc}(C_c)^2C_v - r_{vc-v}(C_cC_{vc}) + \frac{\rho_b}{\theta}r_{v^*c^*-vc}(C_{c^*}C_{v^*c^*}) - r_{vc-v^*c^*}(C_cC_{vc}) - \lambda_{vc}C_cC_{vc} \tag{11}$$

where r_{v-vc} [L^6/M_c^2t] is the rate coefficient of virus attachment onto suspended colloid particles; r_{vc-v} [1/t] is the rate coefficient of virus detachment from suspended colloids; $r_{vc-v^*c^*}$ [1/t] is the rate coefficient of virus–colloid particle attachment onto the solid matrix; and $r_{v^*c^*-vc}$ [1/t] is the rate coefficient of virus–colloid particle detachment from the solid matrix. Finally, the fourth accumulation term on the left hand side of Eq. (9) is given by (Bekhit et al., 2009; Katzourakis and Chrysikopoulos, 2014):

$$\frac{\rho_b}{\theta}\frac{\partial}{\partial t}(C_{c^*}C_{v^*c^*}) = \frac{\rho_b}{\theta}r_{v-v^*c^*}(C_{c^*})^2C_v - \frac{\rho_b}{\theta}r_{v^*c^*-v}(C_{c^*}C_{v^*c^*}) + r_{vc-v^*c^*}(C_cC_{vc}) - \frac{\rho_b}{\theta}r_{v^*c^*-vc}(C_{c^*}C_{v^*c^*}) - \lambda_{v^*c^*}\frac{\rho_b}{\theta}C_{c^*}C_{v^*c^*} \tag{12}$$

where $r_{v-v^*c^*}$ [L^6/M_c^2t] is the rate coefficient of virus attachment onto colloids already attached onto the solid matrix; and $r_{v^*c^*-v}$ [1/t] is the rate coefficient of virus detachment from virus–colloid particles attached onto the solid matrix. Implicitly it is assumed that for colloid facilitated transport the formation of $C_{v^*c^*}$ depends only on $C_{c^*}^{(r)}$, which implies that colloids irreversibly attached onto the solid matrix do not interact with viruses suspended in the aqueous phase. Note that Eqs. (11) and (12) are improved versions of the Eqs. (16) and (20) previously presented by Katzourakis and Chrysikopoulos (2014).

The general functional form of the source configuration is expressed as (Sim and Chrysikopoulos, 1999):

$$F_i(t,x,y,z) = G_i(t)W(x,y,z) \tag{13}$$

where the subscript i represents either colloids (i = c) or viruses (i = v); $G_i(t)$ is the mass release function of species i, with units of [M/t] for a point source and [M/L^3t] for a volume source; and W(x,y,z) characterizes the source physical geometry, with units of [$1/L^3$] for a point source and [–] for an volume source. The mass release rate from a continuous source is given by:

$$G_i(t) = \frac{M_{mr}}{\theta}H(t) \tag{14}$$

where M_{mr} is the mass release rate of species i, with units of [M_i/t] for a point source and [M_i/L^3t] for a volume source; and H(t) [–] is the Heaviside or unit step function (H(t < 0) = 0, H(t ≥ 0) = 1). For a point source geometry, W(x,y,z) is described as follows:

$$W_i(x,y,z) = \delta(x\text{-}x_0)\delta(y\text{-}y_o)\delta(z\text{-}z_0) \tag{15}$$

where x_0, y_0, and z_0 are the Cartesian x-, y-, and z-coordinate locations of the source center, respectively; and $\delta(x\text{-}x_0)$, $\delta(y\text{-}y_0)$, and $\delta(y\text{-}y_0)$, are modified Dirac delta functions (e.g. $\delta = 1$ for $x = x_0$, $\delta = 0$ for $x \neq x_0$). Also, for an ellipsoid source geometry W(x,y,z) is described as follows:

$$W_i(x,y,z) = \begin{cases} 1 & \frac{(x\text{-}x_0)^2}{l_a^2} + \frac{(y\text{-}y_0)^2}{l_b^2} + \frac{(z\text{-}z_0)^2}{l_c^2} \le 1 \\ 0 & \text{otherwise} \end{cases} \tag{16}$$

where l_a, l_b, and l_c are the semi-axes of the ellipsoid parallel to the x-, y-, and z-coordinate directions, respectively.

The initial and boundary conditions for a three-dimensional confined aquifer with finite dimensions are:

$$C_i(0,x,y,z) = 0 \tag{17}$$

$$\frac{\partial^2 C_i(t,0,y,z)}{\partial x^2} = \frac{\partial^2 C_i(t,L_x,y,z)}{\partial x^2} = 0 \tag{18}$$

$$\frac{\partial C_i(t,x,0,z)}{\partial y} = \frac{\partial C_i\left(t,x,L_y,z\right)}{\partial y} = 0 \tag{19}$$

$$\frac{\partial C_i(t,x,y,0)}{\partial z} = \frac{\partial C_i(t,x,y,L_z)}{\partial z} = 0 \tag{20}$$

where L_x, L_y, and L_z [L] are the length, width, and height of the porous medium, respectively. Condition (17) indicates that at the beginning of the simulation no concentration of species i existed within the three-dimensional aquifer. Furthermore the boundary condition (18) preserves concentration continuity at x = 0 and x = L_x (Chrysikopoulos et al., 1990; Shamir and Harleman, 1967). Conditions (19) and (20) establish that the aquifer is impermeable at the lateral and vertical directions,

ensuring that there is no flux of species i across the lateral and vertical boundaries of the confined aquifer. Note that the initial and boundary conditions (17)-(20) are applied to the colloid transport Eq. (1), as well as the virus–colloid cotransport Eq. (9).

3. Numerical solution

Although analytical solutions can be obtained for some relatively complex mathematical models for colloid and contaminant transport in porous media (e.g. Sim and Chrysikopoulos, 1998), the dense-colloid and virus cotransport model presented in this work consists of multiple partial differential equations with complicated source geometries, which can only be solved numerically. Here, the classical and efficient Crank–Nikolson finite differences scheme was implemented. The resulting large system of algebraic equations was solved with the Pardiso package, which is a memory-efficient, and thread-safe software, capable of solving sparse asymmetric and symmetric linear systems of equations (Schenk and Gärtner, 2004). The numerical difficulties that arise with Eqs. (11) and (12), which are "stiff" (equation terms evolve on very different time scales) because the concentration C_c (high frequency component) can take values several orders of magnitude larger than C_{c^*} (low frequency component), were handled with the sophisticated subroutine dodesol (Intel® Ordinary Differential Equations Solver Library), which is capable of solving ordinary differential equations (ODEs) with a variable or a priori unknown stiffness. Note that stiffness can really slow down or even render the solution impossible. Furthermore, it should be noted that the implicit or explicit finite difference scheme was selected automatically by the numerical solution algorithm to ensure that the preselected speed and stability constrains were satisfied. In the presence of stiffness, the implicit scheme was used and the Jacobi numerical matrix was also computed when no analytical alternative was present.

The numerical solution is compared directly with the three-dimensional analytical solution reported by Sim and Chrysikopoulos (1998) for virus transport in an aquifer with finite thickness. The analytical solution was employed for an aquifer with infinite longitudinal and lateral directions and height $L_z = 30$ m, whereas the numerical solution was employed for an aquifer with length $L_x = 100$ m, width $L_y = 30$ m, height $L_z = 30$ m, surrounded by impermeable boundaries. For both cases the contaminant entered the aquifer from a continuous point source, located at $x_0 = 40$ m, $y_0 = 15$ m, $z_0 = 15$ m, having a mass release function $G_v(t) = 1$ mg/h ($t \geq 0$), duration time period of $t_p = 8500$ h, and interstitial velocity was $U_x = 2.5$ cm/h. All other model parameters are listed in Table 2. The simulations shown in Fig. 3 suggest that the analytical and numerical solutions are in perfect agreement.

The numerical solution to the cotransport mathematical model presented here was obtained following the steps outlined by Katzourakis and Chrysikopoulos (2014). The aquifer was discretized into a uniform grid with preselected number of cells so that the relative error between successive iterations was kept lower than 5%. For the simulations presented in this study, the following discretization was used: $n_x = 800$ cells, $n_y = 100$ cells, and $n_z = 100$ cells, for the longitudinal, lateral, and vertical direction, respectively. The various restrictions imposed on the numerical solution are listed in Table 1.

4. Model simulations

For all simulations presented in this work, it is hypothesized that viruses and colloids co-exist in a homogeneous, finite, three-dimensional aquifer with horizontal flow. The aquifer has length $L_x = 100$ m, width $L_y = 30$ m, and height $L_z = 30$ m, and is surrounded with impermeable boundaries. The viruses enter the aquifer from continuous point source, and the colloids from a continuous ellipsoidal shaped source. The virus point source, located at $x_0 = 40$ m, $y_0 = 15$ m, $z_0 = 15$ m, has a mass release function $G_v(t) = 1$ pfu/h ($t \geq 0$), and source geometry function W(x,y,z) described by Eq. (15). Therefore, the virus source configuration is:

$$F_v(t,x,y,z) = 1\ \delta(x\text{-}40)\delta(y\text{-}15)\delta(z\text{-}15)\ \frac{\text{pfu}}{\text{ml}\cdot\text{h}}. \tag{21}$$

The ellipsoid source of colloids has its center located at $x_0 = 6$ m, $y_0 = 15$ m, $z_0 = 15$ m, semi-axes $l_a = 0.4$ m, $l_b = 0.3$ m, $l_c = 0.3$ m, mass release function $G_c(t) = 100$ mg/(ml h) ($t \geq 0$), and source geometry function W(x,y,z) described by Eq. (16). Therefore, the colloid source configuration is:

$$F_c(t,x,y,z) = \begin{cases} 100\ \dfrac{\text{mg}}{\text{ml}\cdot\text{h}} & \dfrac{(x\text{-}6)^2}{0.4^2} + \dfrac{(y\text{-}15)^2}{0.3^2} + \dfrac{(z\text{-}15)^2}{0.3^2} \leq 1 \\ 0 & \text{otherwise} \end{cases}. \tag{22}$$

The horizontal flow is assumed to be aligned with the x-coordinate, which implies that $g_{(\pm i)} = 0$, $g_{(-\mathbf{k})} = -g$, and $U_{cs(\pm i)} = 0$. Also, the colloids are assumed to be spherically shaped with diameter $d_p = 1.4$ μm, and density $\rho_p = 2200$ kg/m^3. Furthermore, the "restricted particle" settling velocity of the dense colloids was estimated with Eq. (2b) using $\rho_w = 998$ kg/m^3, $\mu_w = 0.001$ N·s/m^2, $g = 9.81$ m/s^2, and $f_s = 0.9$ (Wan et al., 1995). All of the model parameters used in the numerical simulations are listed in Table 2.

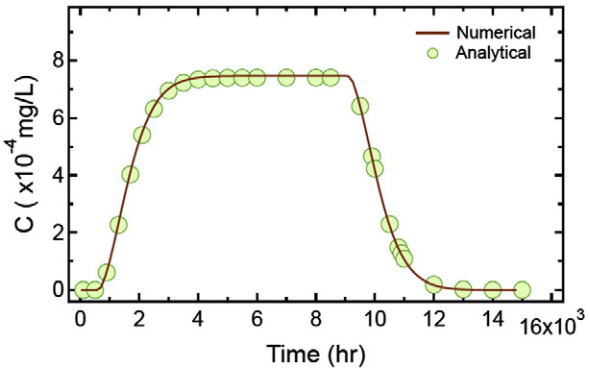

Fig. 3. Comparison of analytical (circles) and numerical solutions (solid curve). Here the duration period of the source is $t_p = 8500$ h, the concentrations are evaluated at $x = 60$ m, $y = 15$ m and $z = 15$ m.

Table 1
Restrictions imposed on the numerical solution.

Number of cells (nx)	500–1000
Temporal discretization step (Δt) [h]	5–10
Spatial discretization step (Δx) [cm]	10–20
Peclet number[a]	<2
Crout number[b]	<1
Main solver relative tolerance[c]	0.05
Relative tolerance between iterations for a particular Δt	10^{-5}
ODE solver relative tolerance	10^{-8}
ODE solver absolute tolerance	10^{-35}

[a] Peclet number: $Pe = U_x\Delta x/D_{xi}$ (Huyakorn and Pinder, 1983).
[b] Courant number: $Cr = U_x\Delta t/\Delta x$ (Zheng and Bennet, 1995).
[c] Successive temporal and spatial discretizations should not produce relative error more than 5%.

In order to better understand how the various model parameters affect C_v, model simulations were performed with fluctuating values of eight different parameters, one at a time. For each of the selected parameters four simulations were performed. The duration of both virus and colloid sources were $t_p = 8500$ h, and C_v concentration histories were predicted at an aquifer location with coordinates x = 50 m, y = 15 m and z = 11 m, based on the parameters values listed in Table 1. The virus and colloid sources are described by Eqs. (21) and (22), respectively. All simulated C_v concentration histories are presented in Fig. 4. Certainly, the C_v concentration histories display higher peaks as the values of D_{xv}, U_x and $r_{c\text{-}c^{*(r)}}$ increase or the values of $r_{v\text{-}v^*}$, U_{cs}, r_{v-vc}, λ_v and λ_{vc} decrease. In general, an increase in C_c causes C_{vc} to increase, and C_v to decrease. Consequently, as shown in Fig. 4e, an increase in $r_{c\text{-}c^{*(r)}}$ causes C_c to decrease and C_v to increase. Fig. 4a suggests that increasing D_{xv} leads to higher peaks, because higher dispersion allows viruses to spread faster. Similarly, decreasing the interstitial velocity reduces the distance that viruses travel over a specific time period, which leads to lower C_v concentrations (see Fig. 4d). Increasing $r_{v\text{-}v^*}$ decreases the C_v concentrations, because more viruses attach on the solid matrix and become immobile (see Fig. 4b). An increase in U_{cs} increases the sedimentation of C_{vc} (note that $U_{cs} = U_{vcs}$), which in turn decreases C_{vc} concentrations at shallow aquifer levels and increases C_{vc} concentrations at deeper aquifer levels (see Fig. 4c). As shown in Fig. 4g,h, increasing either of the parameters λ_v and λ_{vc} leads to decreased C_v. This is because λ_v and λ_{vc} control the inactivation of viruses suspended in the aqueous phase and attached onto suspended colloids, respectively. Note that, if viruses are inactivated faster they are less likely to travel longer distances within the aquifer. Fig. 4f shows that decreasing r_{v-vc} leads to increasing C_v concentrations. This result is expected, because the rate coefficient r_{v-vc} controls virus attachment onto suspended colloid particles. Note that in several of the C_v concentration histories presented in Fig. 4 there is an initial concentration decrease followed by a concentration increase. These concentration peaks are observed at $t > t_p$, or after the colloid and virus sources are eliminated. Consequently, the various concentrations are rearranged due to the absence of colloid and virus sources. Previously attached viruses onto colloids or the aquifer solid matrix shift back into the aqueous phase as suspended viruses, causing a temporary increase in C_v.

Table 2
Model parameters.

Parameter	Value (units)	Reference
Colloid transport parameters		
D_{xc}	30 (cm^2/h)	Schulze-Makuch (2005)
D_{yc}	12 (cm^2/h)	–
D_{zc}	12 (cm^2/h)	–
$r_{c\text{-}c^{*(i)}}$	0.003 (1/h)	Katzourakis and Chrysikopoulos (2014)
$r_{c^{*(r)}\text{-}c}$	0.004 (1/h)	Vasiliadou and Chrysikopoulos (2011)
$r_{c\text{-}c^{*(r)}}$	0.005 (1/h)	Katzourakis and Chrysikopoulos (2014)
U_x	2 (cm/h)	Chrysikopoulos et al. (2012)
U_{cs}	0.4 (cm/h)	Eq. (2a)
Colloid and virus cotransport parameters		
D_{xv}	28 (cm^2/h)	–
D_{yv}	10 (cm^2/h)	–
D_{zv}	10 (cm^2/h)	–
D_{xvc}	30 (cm^2/h)	Schulze-Makuch (2005)
D_{yvc}	12 (cm^2/h)	–
D_{zvc}	12 (cm^2/h)	–
U_{vcs}	0.4 (cm/h)	Eq. (2a)
$r_{v\text{-}v^*}$	0.008 (1/h)	Syngouna and Chrysikopoulos (2011)
$r_{v^*\text{-}v}$	0.005 (1/h)	Vasiliadou and Chrysikopoulos (2011)
$r_{v\text{-}vc}$	27 ($cm^6/mg^2\cdot h$)	–
$r_{vc\text{-}v}$	0.009 (1/h)	Vasiliadou and Chrysikopoulos (2011)
$r_{v\text{-}v^*c^*}$	0.001 ($cm^6/mg^2\cdot h$)	–
$r_{vc\text{-}v^*c^*}$	0.009 (1/h)	Vasiliadou and Chrysikopoulos (2011)
$r_{v^*c^*\text{-}v}$	0.009 (1/h)	Vasiliadou and Chrysikopoulos (2011)
$r_{v^*c^*\text{-}vc}$	0.05 (1/h)	Vasiliadou and Chrysikopoulos (2011)
λ_v	0.001 (1/h)	Syngouna and Chrysikopoulos (2011)
λ_{v^*}	0.0005 (1/h)	Syngouna and Chrysikopoulos (2011)
λ_{vc}	0.0001 (1/h)	Syngouna and Chrysikopoulos (2011)
$\lambda_{v^*c^*}$	0.00005 (1/h)	Syngouna and Chrysikopoulos (2011)

To illustrate the effects of gravity during field-scale cotransport of viruses and dense colloids, multiple model simulations were performed. Fig. 5 presents contour plots for concentrations C_v, C_c, and C_{vc} at a single time frame (t = 6900 h), as predicted by the cotransport model. The results clearly show that all three concentrations (C_c, C_v, and C_{vc}) are affected by gravity. Although viruses are assumed to have no "restricted particle" settling, the C_v contours are influenced by gravity. Certainly, this is not an intuitive result, because it is attributed to virus attachment onto dense colloids, followed by subsequent virus detachment from colloid surfaces into the aqueous phase. To better illustrate the effect of gravity on the virus and dense colloid cotransport in porous media, a series of C_v, C_c, and C_{vc} contour snapshots, at six different times (t = 150, 1050, 2100, 3000, 5700 and 6900 h), are presented in Fig. 6. As expected, due to the high density of the colloids, the contours for both C_c, and C_{vc} are affected by gravity. Initially, viruses are transported along the horizontal flow, but after they encounter the colloid source at x = 4000 cm, they bend towards the bottom of the aquifer. When viruses interact with the colloid particles, virus–colloid particles are formed, which due to their "restricted" settling velocity, they are transported in a downward direction, where they are allowed to detach from each other and to yield a local virus concentration, essentially virus transport is enhanced. Note that as time elapses, the effect of gravity is more pronounced (see concentration contour snapshots in Fig. 6).

For direct comparison, a second set of model simulations were performed with the results presented in Fig. 7, by employing identical flow conditions and parameter values to those used for the construction of Fig. 6, with the exception that

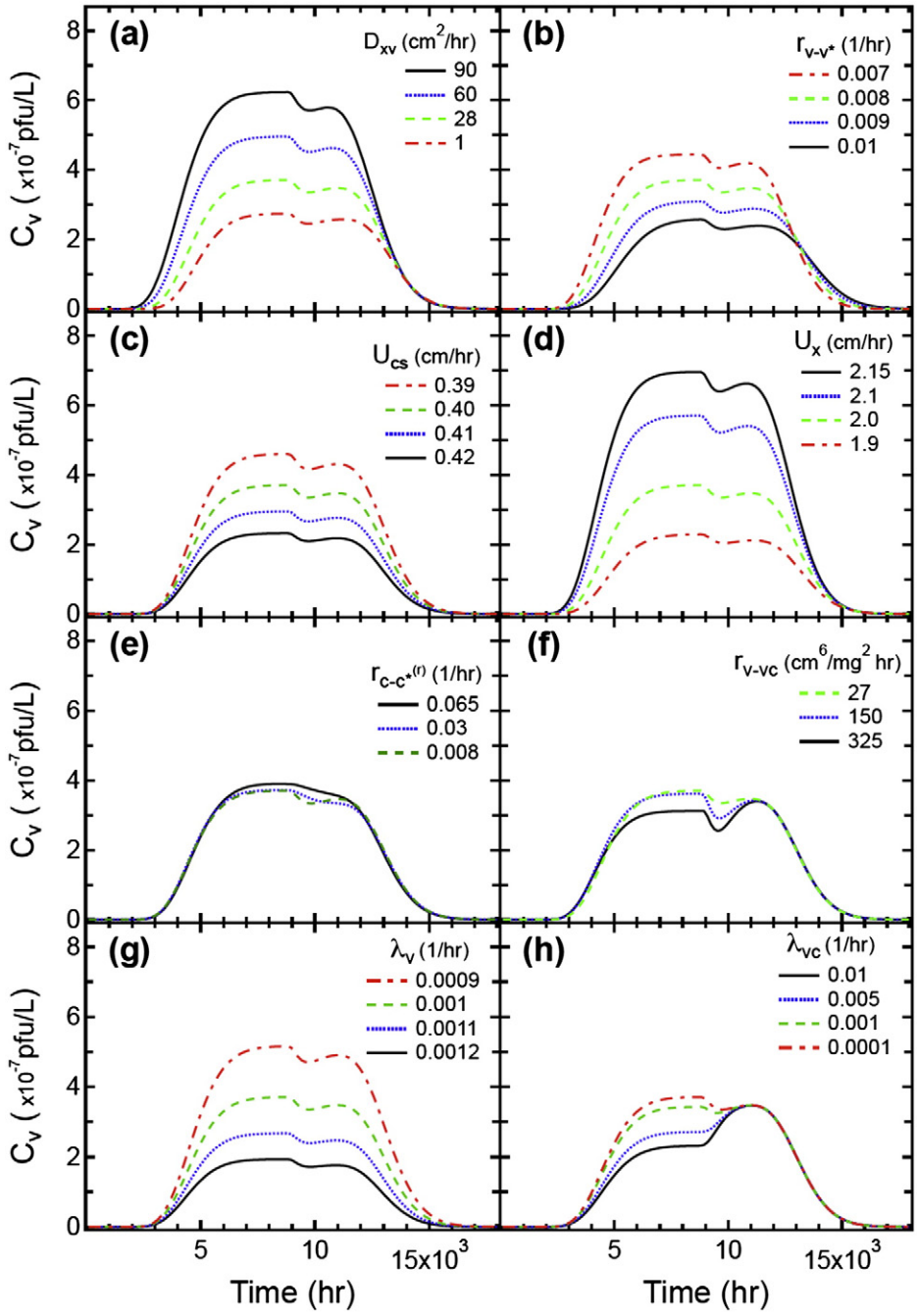

Fig. 4. Sensitivity analysis on various parameters of the newly developed virus–dense colloid cotransport model. Here $t_p = 8500$ h.

this time gravity effects were thought to be negligible for both virus and colloid particles. Clearly, the contour snapshots shown in Fig. 7 illustrate that all three concentrations (C_c, C_v, and C_{vc}) are no longer affected by gravity. However, low virus concentration zones still exist within the contours, due to the formation of virus–colloid particles.

Finally, for better visualization of the virus and colloid spatial distributions within the hypothetical, three-dimensional aquifer examined in this work, iso-surface plots were created. Fig. 8 presents iso-surface plots for both C_v, and C_{vc}, as well as concentration contours for C_c, for the same flow conditions and parameter values used for the construction of Fig. 6, were gravity effects are accounted by the cotransport model. As expected, downstream from the colloid source there is a region of low virus concentration (virus transport is hindered), created by the formation of virus–colloid particles. Clearly, the vertical migration of viruses is caused by the presence of dense colloid particles (virus transport is enhanced).

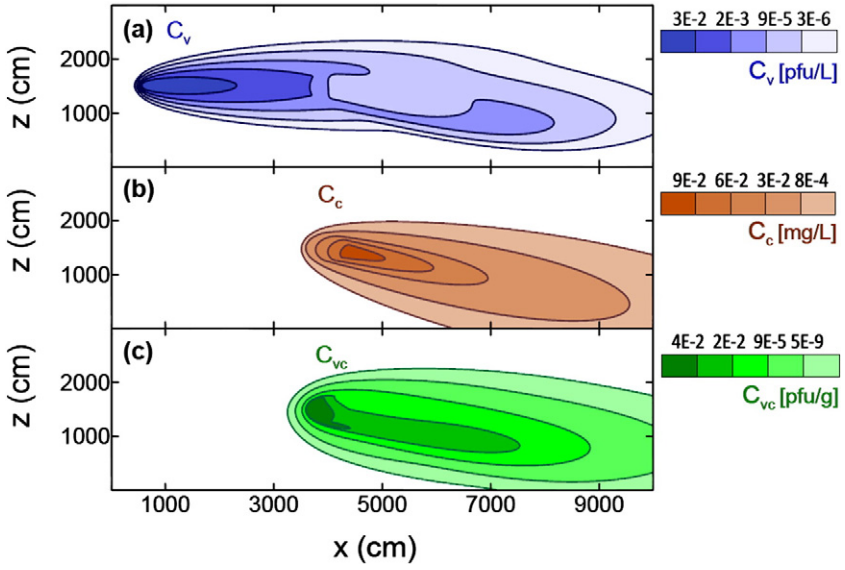

Fig. 5. Concentration contour plots on the x–z plane for: (a) viruses, (b) colloids, and (c) virus–colloid particles during virus and colloid cotransport, accounting for gravitational effects. Here t = 6900 h, and y = 15 m.

5. Summary

A mathematical model describing the cotransport of viruses and colloids in three-dimensional, homogeneous, water saturated porous media, accounting for gravity effects was developed. The numerical solution was implemented with the use of implicit and non-implicit finite difference procedures, as well as ODE solvers, which efficiently handled variable or a priori unknown stiffness. Multiple model simulations were performed for the cotransport of virus and dense colloid particles in a hypothetical aquifer, using parameter values reported in the literature. The results demonstrated that the presence of dense colloids influence the transport of viruses in porous media. Certainly, the cotransport model and its numerical solution presented in this work can easily be applied to other types of biocolloids/contaminants and dense colloids (nanomaterials).

Nomenclature

b	ratio of average free settling segment length to the grain radius, (–).
C_c	concentration of suspended colloids, M_c/L^3.
C_i	concentration of suspended species i, M_c/L^3, M_v/L^3, M_v/M_c.
C_c^*	concentration of colloids attached onto the solid matrix, M_c/M_s.
C_v	concentration of suspended viruses, M_v/L^3.
C_v^*	concentration of viruses attached onto the solid matrix, M_v/M_s.
C_{vc}	concentration of viruses attached onto suspended colloid particles, M_v/M_c.
$C_{v^*c^*}$	concentration of virus–colloid particles attached onto the solid matrix, M_v/M_c.
$C_{c^*}^{(i)}$	concentration of colloids irreversibly attached onto the solid matrix, M_c/M_s.
$C_{c^*}^{(r)}$	concentration of colloids reversibly attached onto the solid matrix, M_c/M_s.
d_p	colloid particle diameter, L.
D_{xi}	longitudinal hydrodynamic dispersion coefficient of species i, L^2/t.
D_{yi}	lateral hydrodynamic dispersion coefficient of species i, L^2/t.
D_{zi}	vertical hydrodynamic dispersion coefficient of species i, L^2/t.
f_s	settling velocity correction factor, (–).
F_i	general form of the source configuration of species i, M_i/L^3t.
g	gravitational acceleration, L/t^2.
$G_i(t)$	mass release function of species i, point source: M_i/t, and volume source: M_i/L^3t.
H(t)	Heaviside or unit step function ($H(t < 0) = 0$, $H(t \geq 0) = 1$), (–).
i	species c = colloid, v = virus, vc = virus–colloid.
l_a	ellipsoid semi-axis parallel to the x-direction, L.
l_b	ellipsoid semi-axis parallel to the y-direction, L.
l_c	ellipsoid semi-axis parallel to the z-direction, L.
L	length, L.
L_x	length of porous medium (packed column), L.
L_y	width of porous medium, L.
L_z	height of porous medium, L.
M	mass, M.
M_c	mass of colloids, M_c.
M_s	mass of the solid matrix, M_s.
M_v	mass of viruses, M_v.
M_{mr}	mass release rate of species i, point source: M_i/t, and volume source: M_i/L^3t.
n_x	number of discretization unit cells in the x-direction, (–).
$r_{c\text{-}c^{*(i)}}$	rate coefficient of irreversible colloid attachment onto the sold matrix, 1/t.

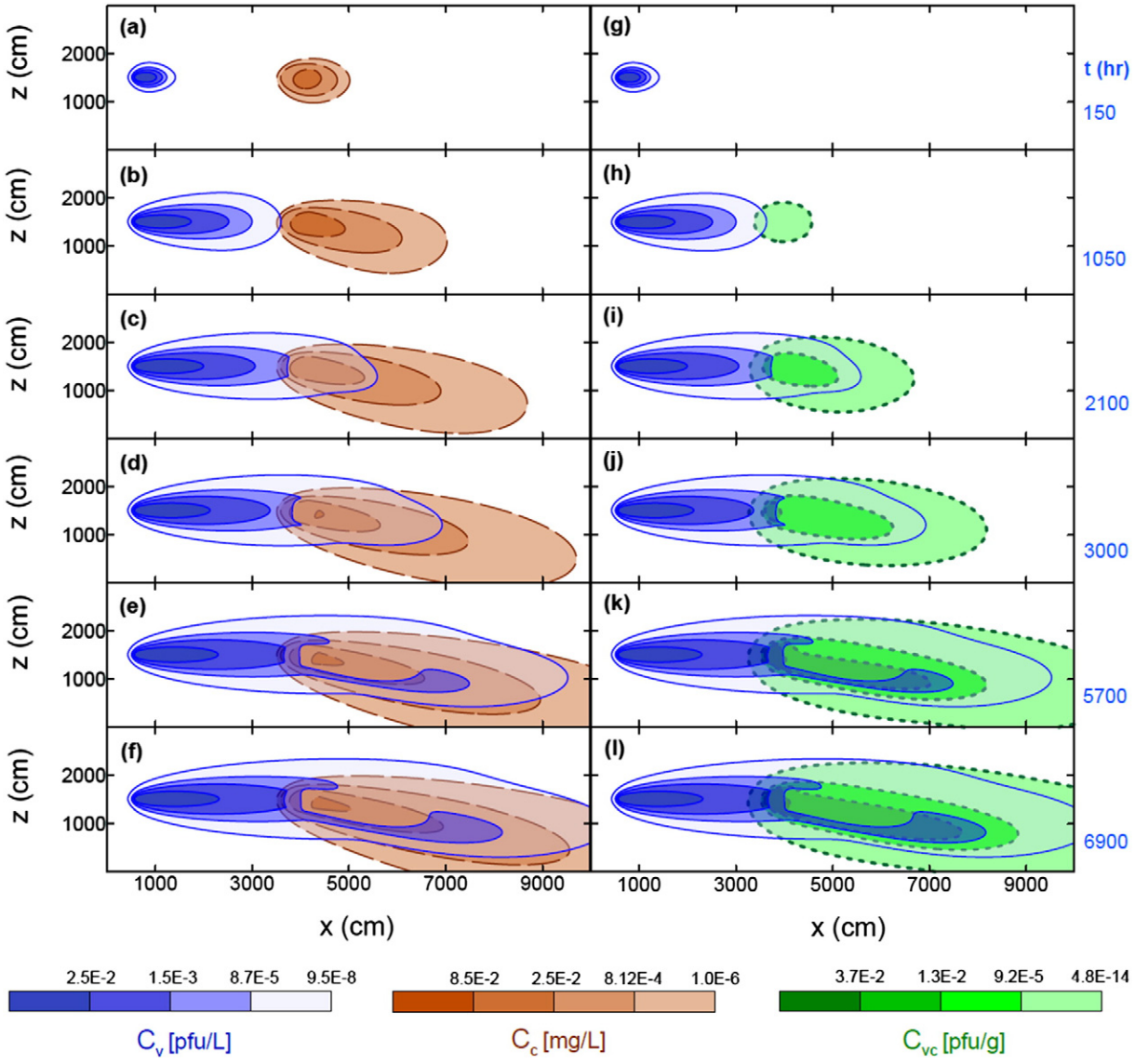

Fig. 6. Contour plots on the x–z plane for: (a–f) viruses (solid curves) and colloid particles (dashed curves), and (g–l) viruses (solid curves) and virus–colloid particles (dotted curves) during virus and colloid cotransport in the presence of gravitational effects. Here (a,g) t = 150 h, (b,h) t = 1050 h, (c,i) t = 2010 h, (d,j) t = 3000 h, (e,k) t = 5700 h, (f,l) t = 6900 h, and y = 15 m.

$r_{c\text{-}c^{*(r)}}$	rate coefficient of reversible colloid attachment onto the sold matrix, 1/t.
$r_{c^{*(r)}\text{-}c}$	rate coefficient of reversible colloid detachment from the solid matrix, 1/t.
$r_{v\text{-}v^*}$	rate coefficient of virus attachment onto the solid matrix, 1/t.
$r_{v^*\text{-}v}$	rate coefficient of virus detachment from the solid matrix, 1/t.
$r_{v\text{-}vc}$	rate coefficient of virus attachment onto suspended colloid particles, L^6/M_c^2t.
$r_{vc\text{-}v}$	rate coefficient of virus detachment from suspended colloid particles, 1/t.
$r_{v\text{-}v^*c^*}$	rate coefficient of virus attachment onto colloid particles already attached onto the solid matrix, L^6/M_c^2t.
$r_{vc\text{-}v^*c^*}$	rate coefficient of virus–colloid particle attachment onto the solid matrix,1/t.
$r_{v^*c^*\text{-}v}$	rate coefficient of virus detachment from colloid particles attached onto the solid matrix, 1/t.
$r_{v^*c^*\text{-}vc}$	rate coefficient of virus–colloid particle detachment from the solid matrix, 1/t.
t	time, t.
t_p	source duration time period, t.
U_x	interstitial velocity in the x-direction, L/t.
$U_{is(\pm\mathbf{i})}$	x-directional component of the restricted settling velocity of species i, L/t.
$U_{is(-\mathbf{k})}$	negative z-directional component of the restricted settling velocity of species i, L/t.
W	characterizes the source physical geometry, point source: $1/L^3$, volume source: (−).

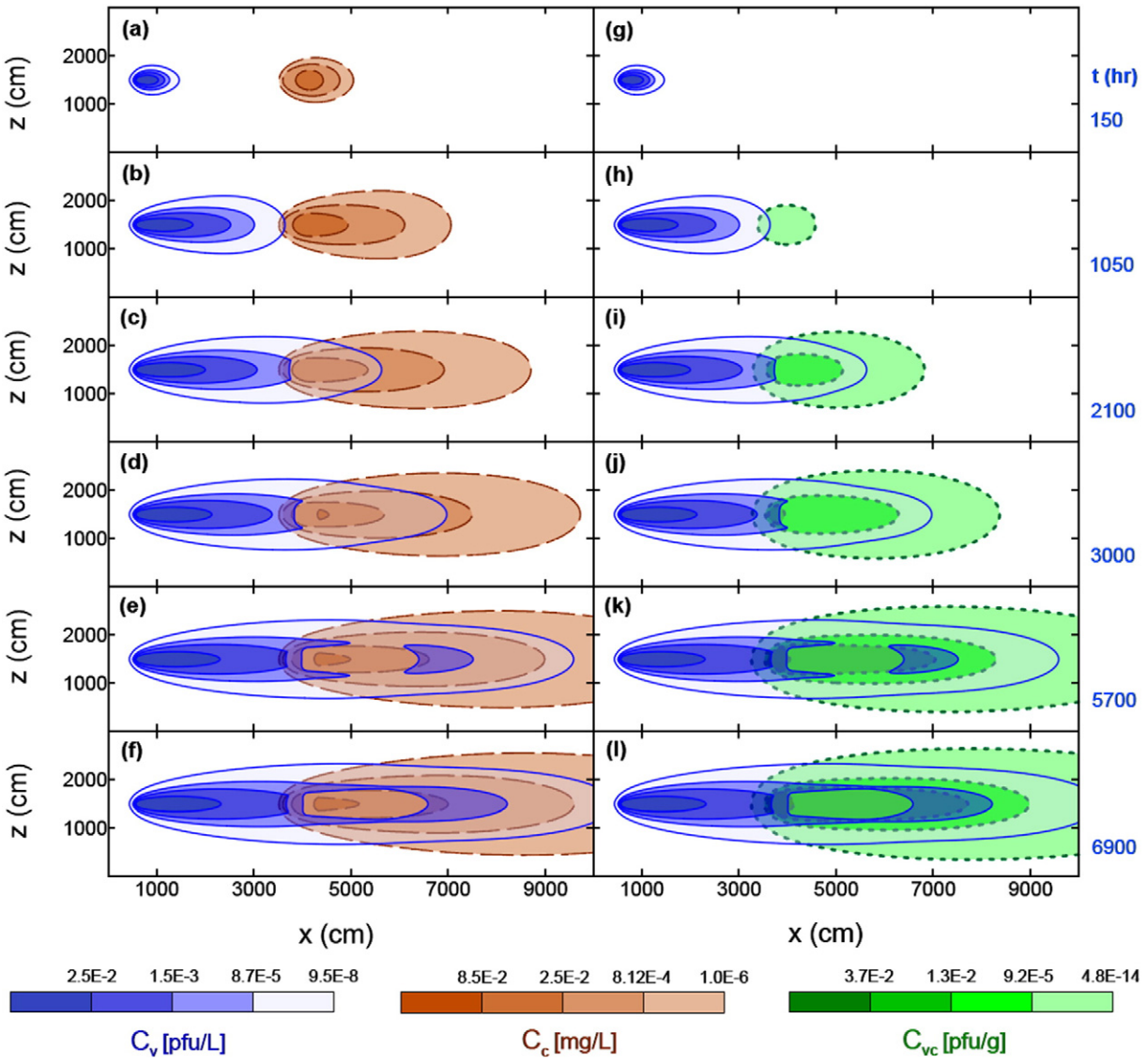

Fig. 7. Contour plots on the x–z plane for: (a–f) viruses (solid curves) and colloid particles (dashed curves), and (g–l) viruses (solid curves) and virus–colloid particles (dotted curves) during virus and colloid cotransport in the absence of gravitational effects. Here (a,g) t = 150 h, (b,h) t = 1050 h, (c,i) t = 2010 h, (d,j) t = 3000 h, (e,k) t = 5700 h, (f,l) t = 6900 h, and y = 15 m.

x	Cartesian coordinate in the longitudinal direction, L.
x_0	Cartesian x-coordinate location of the source center, L.
y	Cartesian coordinate in the lateral direction, L.
y_0	Cartesian y-coordinate location of the source center, L.
z	Cartesian coordinate in the vertical direction, L.
z_0	Cartesian z-coordinate location of the source center, L.

Greek Letters

β	angle of the main flow direction (x-direction) with respect to the direction of gravity.
ε	empirical correction factor, (–).
δ	modified Dirac delta function, 1/L.
θ	porosity of the column material, (L^3 voids)/(L^3 solid matrix).
μ_w	dynamic viscosity of water, M/(L·t).
λ_v	decay rate of viruses suspended in the liquid phase, 1/t.
λ_v^*	decay rate of viruses sorbed or attached onto the solid matrix, 1/t.
λ_{vc}	decay rate of virus–colloid complexes suspended in the liquid phase, 1/t.
$\lambda_{v^*c^*}$	decay rate of virus–colloid complexes sorbed or attached onto the solid matrix, 1/t.
ρ_b	bulk density of the solid matrix, M_s/L^3.
ρ_p	particle density, M/L^3.
ρ_w	fluid density, M/L^3.

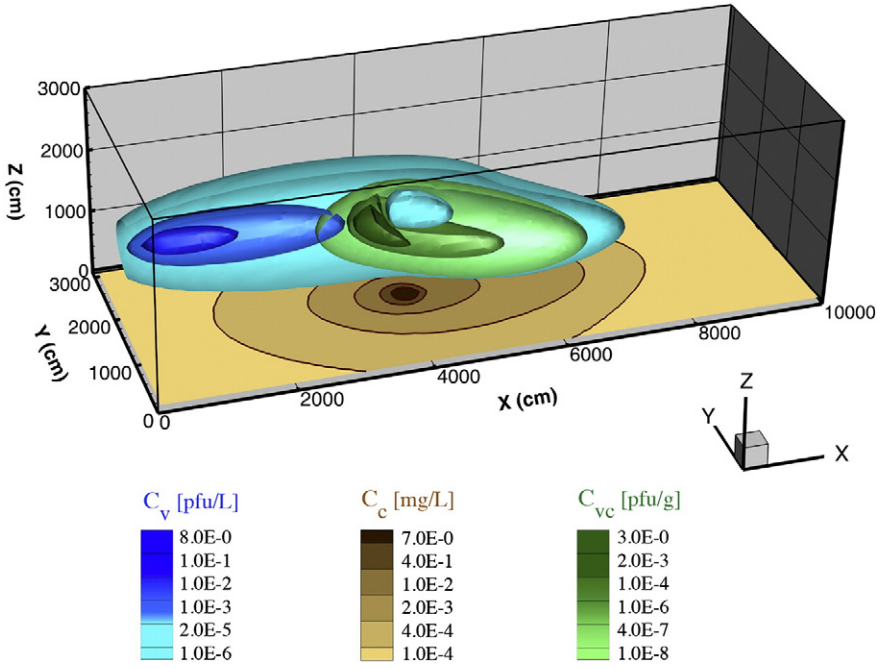

Fig. 8. Isosurface three-dimensional concentrations plots for viruses (blue surfaces) and virus–colloid particles (green surfaces), along with a projected contour plot on the x–y plane at z = 15 m for colloid particles (brown contour). Here t = 13,000 h.

Abreviations

ODE	ordinary differential equation
PDE	partial differential equation

Acknowledgments

This research has been co-financed by the European Union (European Social Fund-ESF) and Greek National Funds through the Operational program "Education and Lifelong Learning" under the action Aristeia I (Code No. 1185).

References

Abdel-Salam, A., Chrysikopoulos, C.V., 1995a. Modeling of colloid and colloid-facilitated contaminant transport in a two-dimensional fracture with spatially variable aperture. Transp. Porous Media 20 (3), 197–221. http://dx.doi.org/10.1007/BF01073172.

Abdel-Salam, A., Chrysikopoulos, C.V., 1995b. Analysis of a model for contaminant transport in fractured media in the presence of colloids. J. Hydrol. 165, 261–281. http://dx.doi.org/10.1016/0022-1694(94)02675-2.

Anders, R., Chrysikopoulos, C.V., 2005. Virus fate and transport during artificial recharge with recycled water. Water Resour. Res. 41 (10), W10415. http://dx.doi.org/10.1029/2004WR003419.

Anders, R., Chrysikopoulos, C.V., 2006. Evaluation of the factors controlling the time-dependent inactivation rate coefficients of bacteriophage MS2 and PRD1. Environ. Sci. Technol. 40 (10), 3237–3242. http://dx.doi.org/10.1021/es051604b.

Anders, R., Chrysikopoulos, C.V., 2009. Transport of viruses through saturated and unsaturated columns packed with sand. Transp. Porous Media 76, 121–138. http://dx.doi.org/10.1007/s11242-008-9239-3.

Artinger, R., Rabung, T., Kim, J.I., Sachs, S., Schmeide, K., Heise, K.H., Bernhard, G., Nitsche, H., 2002. Humic colloid-borne migration of uranium in sand columns. J. Contam. Hydrol. 58, 1–12.

Bekhit, H.M., El-Kordy, M.A., Hassan, A.E., 2009. Contaminant transport in groundwater in the presence of colloids and bacteria. Model development and verification. J. Contam. Hydrol. 108, 152–167.

Bradford, S.A., Torkzaban, S., Simunek, J., 2011. Modeling colloid transport and retention in saturated porous media under unfavorable attachment conditions. Water Resour. Res. 47, W10503. http://dx.doi.org/10.1029/2011WR010812.

Chen, X.-X., Bai, B., 2012. Effect of gravity on transport of particles in saturated porous media. Chin. J. Geotech. Eng. 34 (9), 1661–1667.

Chen, G., Hong, Y., Walker, S.L., 2010. Colloidal and bacterial deposition: role of gravity. Langmuir 26, 314–319.

Chrysikopoulos, C.V., Aravantinou, A.F., 2012. Virus inactivation in the presence of quartz sand under static and dynamic batch conditions at different temperatures. J. Hazard. Mater. 233–234, 148–157. http://dx.doi.org/10.1016/j.jhazmat.2012.07.002.

Chrysikopoulos, C.V., Sim, Y., 1996. One-dimensional virus transport homogeneous porous media with time dependent distribution coefficient. J. Hydrol. 185, 199–219. http://dx.doi.org/10.1016/0022-1694(95)02990-7.

Chrysikopoulos, C.V., Aravantinou, A.F., 2014. Virus attachment onto quartz sand: Role of grain size and temperature. J. Environ. Chem. Eng. 2, 796–801. http://dx.doi.org/10.1016/j.jece.2014.01.025.

Chrysikopoulos, C.V., Syngouna, V.I., 2014. Effect of gravity on colloid transport through water-saturated columns packed with glass beads: modeling and experiments. Environ. Sci. Technol. 48, 6805–6813. http://dx.doi.org/10.1021/es501295n.

Chrysikopoulos, C.V., Roberts, P.V., Kitanidis, P.K., 1990. One-dimensional solute transport in porous media with partial well-to-well recirculation: application to field experiments. Water Resour. Res. 26 (6), 1189–1195. http://dx.doi.org/10.1029/89WR03629.

Chrysikopoulos, C.V., Masciopinto, C., La Mantia, R., Manariotis, I.D., 2010. Removal of biocolloids suspended in reclaimed wastewater by injection in a fractured aquifer model. Environ. Sci. Technol. 44 (3), 971–977. http://dx.doi.org/10.1021/es902754n.

Chrysikopoulos, C.V., Syngouna, V.I., Vasiliadou, I.A., Katzourakis, V.E., 2012. Transport of Pseudomonas putida in a three-dimensional bench scale experimental aquifer. Transp. Porous Media 94, 634–635. http://dx.doi.org/10.1007/s11242-012-0015-z.

Chu, Y., Jin, Y., Baumann, T., Yates, M.V., 2003. Effect of soil properties on saturated and unsaturated virus transport through columns. J. Environ. Qual. 32, 2017–2025.

Compere, F., Porel, G., Delay, F., 2001. Transport and retention of clay particles in saturated porous media: influence of ionic strength and pore velocity. J. Contam. Hydrol. 49, 1–21.

Craun, G.F., Brunkard, J.M., Yoder, J.S., Roberts, V.A., Carpenter, J., Wade, T., Calderon, R.L., Roberts, J.M., Beach, M.J., Roy, S.L., 2010. Causes of outbreaks

associated with drinking water in the United States from 1971 to 2006. Clin. Microbiol. Rev. 23 (3), 507–528.
Flowers, T.C., Hunt, J.R., 2007. Viscous and gravitational contributions to mixing during vertical brine transport in water-saturated porous media. Water Resour. Res. 43, Wo1407. http://dx.doi.org/10.1029/2005WR004773.
Gschwend, P.M., Backhus, D.A., MacFarlane, J.K., Page, A.L., 1990. Mobilization of colloids in groundwater due to infiltration of water at a coal ash disposal site. J. Contam. Hydrol. 6, 307–320.
Harvey, R.W., Garabedian, S.P., 1991. Use of colloid filtration theory in modeling movement of bacteria through a contaminated sandy aquifer. Environ. Sci. Technol. 25, 178–185.
Huyakorn, P.S., Pinder, G.F., 1983. Computational Methods in Subsurface Flow. Academic Press, San Diego.
James, S.C., Bilezikjian, T.K., Chrysikopoulos, C.V., 2005. Contaminant transport in a fracture with spatially variable aperture in the presence of monodisperse and polydisperse colloids. Stochastic Environ. Res. Risk Assess. 19 (4), 266–279. http://dx.doi.org/10.1007/s00477-004-0231-3.
Jin, Y., Yates, M.V., Thompson, S.S., Jury, W.A., 1997. Sorption Interactions and survival of enteric viruses in soil materials. Environ. Sci. Technol. 31, 548–555.
Katzourakis, V.E., Chrysikopoulos, C.V., 2014. Mathematical modeling of colloid and virus cotransport in porous media. Adv. Water Resour. 68, 62–73. http://dx.doi.org/10.1016/j.advwatres.2014.03.001.
Kim, H.N., Bradford, S.A., Walker, S.L., 2009. Escherichia coli O157:H7 transport in saturated porous media: role of solution chemistry and surface macromolecules. Environ. Sci. Technol. 43, 4340–4347.
Kretzschmar, R., Borkovec, M., Grolimund, D., Elimelech, M., 1999. Mobile subsurface colloids and their role in contaminant transport. Adv. Agron. 66, 121–194.
Ma, H., Pazmino, E.F., Johnson, W.P., 2011. Gravitational settling effects on unit cell predictions of colloidal retention in porous media in the absence of energy barriers. Environ. Sci. Technol. 45, 8306–8312.
Masciopinto, C., La Mantia, R., Chrysikopoulos, C.V., 2008. Fate and transport of pathogens in a fractured aquifer in the Salento area, Italy. Water Resour. Res. 44 (1), W01404. http://dx.doi.org/10.1029/2006WR005643.
McCarthy, J.F., 1998. Colloid-facilitated transport of contaminants in groundwater: mobilization of transuranic radionuclides from disposal trenches by natural organic matter. Phys. Chem. Earth 23, 171–178.
McGechan, M.B., Lewis, D.R., 2002. Transport of particulate and colloid sorbed contaminants through soil: Part 1. General principles. Biosyst. Eng. 83, 255–273.
Mibus, J., Sachs, S., Pfingsten, W., Nebelung, C., Bernhard, G., 2007. Migration of uranium (IV)/(VI) in the presence of humic acids in quartz sand: a laboratory column study. J. Contam. Hydrol. 89, 199–217.
Ouyang, Y., Shinde, D., Mansell, R.S., Harris, W., 1996. Colloid enhanced transport of chemicals in subsurface environments: a review. Crit. Rev. Environ. Sci. Technol. 26, 189–204.
Park, N., Blanford, T.N., Huyakorn, P.S., 1992. VIRALT: A Modular Semi-analytical and Numerical Model for Simulating Viral Transport in Ground Water. International Ground Water Modeling Center, Colorado School of Mines, Golden, CO.
Russel, W.B., Saville, D.A., Schowlter, W.R., 1989. Colloidal Dispersions. Cambridge University Press, Cambridge, UK (525 pp.).
Saiers, J.E., Hornberger, G.M., 1996. The role of colloidal kaolinite in the transport of cesium through laboratory sand columns. Water Resour. Res. 32 (1), 33–41.
Schenk, O., Gärtner, K., 2004. Solving unsymmetric sparce systems of linear equations with PARADISO. J. Futur. Gener. Comput. Syst. 20 (3), 475–487.
Schulze-Makuch, D., 2005. Longitudinal dispersivity data and implications for scaling behavior. Ground Water 43 (3), 443–456.
Sen, T.K., Khilar, K.C., 2006. Review on subsurface colloids and colloid-associated contaminant transport in saturated porous media. Adv. Colloid Interf. Sci. 119, 71–96.
Severino, G., Cvetkovic, V., Coppola, A., 2007. Spatial moments for colloid-enhanced radionuclide transport in heterogeneous aquifers. Adv. Water Resour. 30, 101–112.
Shamir, U.Y., Harleman, D.R.F., 1967. Numerical solutions for dispersion in porous mediums. Water Resour. Res. 3 (2), 557–581.
Sim, Y., Chrysikopoulos, C.V., 1995. Analytical models for one-dimensional virus transport in saturated porous media. Water Resour. Res. 31 (5), 1429–1437. http://dx.doi.org/10.1029/95WR00199 (Correction, 1996a. Water Resour. Res., 32(5), 1473, doi:10.1029/96WR00675.).
Sim, Y., Chrysikopoulos, C.V., 1996. One-dimensional virus transport in porous media with time dependent inactivation rate coefficients. Water Resour. Res. 32 (8), 2607–2611. http://dx.doi.org/10.1029/96WR01496.
Sim, Y., Chrysikopoulos, C.V., 1998. Three-dimensional analytical models for virus transport in saturated porous media. Transp. Porous Media 30, 87–112. http://dx.doi.org/10.1023/A:1006596412177.
Sim, Y., Chrysikopoulos, C.V., 1999. Analytical solutions for solute transport in saturated porous media with semi-infinite or finite thickness. Adv. Water Resour. 22 (5), 507–519. http://dx.doi.org/10.1016/S0309-1708(98)00027-X.
Sim, Y., Chrysikopoulos, C.V., 2000. Virus transport in unsaturated porous media. Water Resour. Res. 36 (1), 173–179. http://dx.doi.org/10.1029/1999WR900302.
Syngouna, V.I., Chrysikopoulos, C.V., 2011. Transport of biocolloids in water saturated columns packed with sand: effect of grain size and pore water velocity. J. Contam. Hydrol. 126, 301–314. http://dx.doi.org/10.1016/j.jconhyd.2011.09.007.
Syngouna, V.I., Chrysikopoulos, C.V., 2013. Cotransport of clay colloids and viruses in water saturated porous media. Colloids Surf. A Physicochem. Eng. Asp. 416, 56–65. http://dx.doi.org/10.1016/j.colsurfa.2012.10.018.
Syngouna, V.I., Chrysikopoulos, C.V., 2015. Experimental investigation of virus and clay particles cotransport in partially saturated columns packed with glass beads. J. Colloid Interface Sci. 440, 140–150. http://dx.doi.org/10.1016/j.jcis.2014.10.066.
Tatalovich, M.E., Lee, K.Y., Chrysikopoulos, C.V., 2000. Modeling the transport of contaminants originating from the dissolution of DNAPL pools in aquifers in the presence of dissolved humic substances. Transp. Porous Media 38 (1/2), 93–115. http://dx.doi.org/10.1023/A:1006674114600.
Tim, U.S., Mostaghimi, S., 1991. Model for predicting virus movement through soils. Ground Water 29 (2), 251–259.
Torkzaban, S., Bradford, S.A., Th, M., van Genuchten, and S.L. Walker, 2008. Colloidtransport in unsaturated porous media: the role of water content and ionicstrength on particle straining. J. Contam. Hydrol. 96, 113–127.
Vasiliadou, I.A., Chrysikopoulos, C.V., 2011. Cotransport of *Pseudomonas putida* and kaolinite particles through water saturated columns packed with glass beads. Water Resour. Res. 47, W02543. http://dx.doi.org/10.1029/2010WR009560.
Villholth, K.G., Jarvis, N.J., Jacobsen, O.H., de Jonge, H., 2000. Field investigations and modeling of particle-facilitated pesticide transport in microporous soil. J. Environ. Qual. 29, 1298–1309.
Walshe, G.E., Pang, L., Flury, M., Close, M.E., Flintoft, M., 2010. Effects of pH, ionic strength, dissolved organic matter, and flow rate on the cotransport of MS2 bacteriophages with kaolinite in gravel aquifer media. Water Res. 44, 1255–1269.
Wan, J., Tokunaga, T., Tsang, C., 1995. Bacterial sedimentation through a porous medium. Water Resour. Res. 31 (7), 1627–1636.
Zheng, C., Bennet, G.D., 1995. Applied Contaminant Transport Modeling. Van Nostrand Reinhold ITP, New York.